J Therm Anal Calorim (2010) 102:69–74
DOI 10.1007/s10973-009-0630-2

Characterization of anticancer hypocrellin A encapsulated with silica nanoparticles

Thermal analysis

Fang Wang · Lin Zhou · Jiahong Zhou · Xiaotian Gu · Yuying Feng

Received: 25 August 2009 / Accepted: 2 December 2009 / Published online: 5 January 2010

Abstract Hypocrellins, natural photosensitizers including hypocrellin A (HA) and hypocrellin B (HB), have been used as a traditional Chinese herbal medicine to cure various skin diseases. Hypocrellins have excellent antiviral activity, which can inhibit the growth of human immunodeficiency virus. They also exhibit significant light-induced antitumor property. In this article, thermal analysis technologies (e.g., differential scanning calorimetry and thermogravimetry) are employed to characterize whether the photosensitive hypocrellin A could be encapsulated with silica nanoparticle (SN) material or not, and evaluate the stability of inclusion complex. The results show that the inclusion complex exhibits improved performance in both stability and hydrophilicity than natural hypocrellin A. Fluorescence spectrophotometry studies have also been performed to verify the thermal analysis results. The results suggest that the thermal analysis technology could be used as an effective and rapid tool to characterize the encapsulation properties of the novel anticancer HA–SN complex.

Keywords Hypocrellin · Silica nanoparticle · Differential scanning calorimetry · Thermogravimetry

F. Wang (✉) · L. Zhou · J. Zhou · X. Gu · Y. Feng
Analysis and Testing Center, Nanjing Normal University, 210097 Nanjing, Jiangsu, China
e-mail: wangfang@njnu.edu.cn

F. Wang · J. Zhou · X. Gu · Y. Feng
Jiangsu Testing Service Center for Biomedicinal Materials, Nanjing Normal University, 210097 Nanjing, Jiangsu, China

L. Zhou
Complex Presection of CMM, China Pharmaceutical University, 210038 Nanjing, Jiangsu, China

Introduction

Hypocrellins (hypocrellin A and B, referred to as HA and HB, as shown in Fig. 1) are some natural photosensitizers (PS). They can be extracted from *Hypocrella bambuase*, and have been used as a valuable traditional Chinese herbal medicine to cure various skin diseases [1]. The hypocrelline have excellent antiviral activity to inhibit the growth of the human immunodeficiency virus. Recently, these natural perylenequinoid compounds have been observed to exhibit significant light-induced antitumor and antiviral activities, especially for human immunodeficiency virus (HIV). Some novel advantages of Hypocrellins were reported, such as easy preparation and purification, strong infrared light absorptivity, high quantum yields of singlet oxygen, rapid metabolism in vivo, and nearly no dark toxicity etc. [2, 3]. Therefore, hypocrellins are suggested to have great potential in the development of new generation photodynamic therapy (PDT) drug.

The wavelength range of PDT for malignant tumor in clinic should be 600–900 nm and the penetration depth is about several mm to 1 cm. However, the central absorptive wavelength of nature HA is just close to 500 nm and the penetration depth is only 1 mm, which cannot satisfy the requirement of PDT. In recent years, hypocrellin-related researches have been focused on how to extend the absorptive wavelength range of HA, as well as the mechanism of the antitumor activity [4–8]. However, as an anticancer PDT medicine, hyprocrellins always tend to aggregate into clusters in blood to block the vessels because of the relatively lower water insolubility, so that it is difficult to deliver the pharmaceutic formulations to the desire area. In other words, the major obstacle to the PDT development of hyprocrellins is their poor water solubility. In order to solve this problem, porous hollow silica

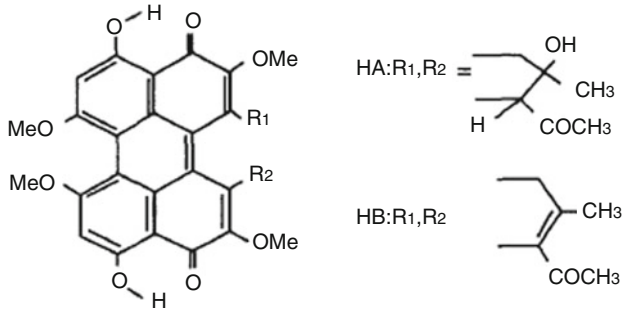

Fig. 1 Molecular structure of hypocrellin

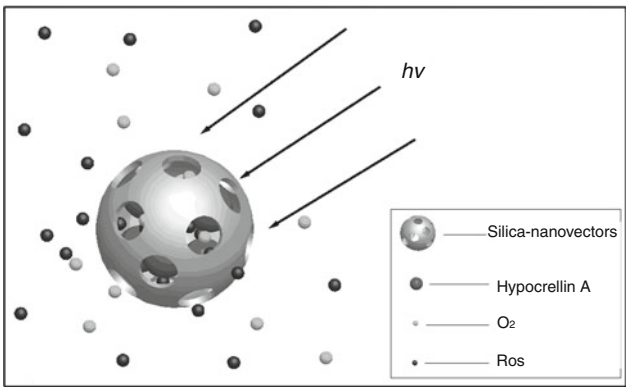

Fig. 2 Photosensitive dynamic schematic of HA–SNs (HA-silica nanoparticles)

nanoparticles (SNs) were developed in this study as carriers for photosensitive drug delivery. Inclusion complexes, hypocrellin A-silica nanoparticles (HA–SNs) are compounded by encapsulating HA in the shell of SN. Comparing with conventional drug delivery systems, SNs with the porous shell structure will allow the active oxygen species produced from photosensitizing drug HA to permeate easily through the pores in the shell, without releasing the photosensitive drugs themselves [9, 10] (as shown in Fig. 2).

Considering phototoxic side effects which might be induced if the photosensitive drugs were adhered on the external shell surface of SN, it is necessary to verify whether the photosensitive drug HAs are encapsulated in the shell or just adhered on the external surface of shell. Thus, this study aimed at developing a fast and effective technology to characterize the anticancer drug HA–SN, which is very important for improving the development of HA-related PDT drugs.

Thermal analysis techniques are modern analytical methods that were developed rapidly with the development of micro-quality and microcomputer technology since 1980s. This kind of method was first used in biological and medical researches [11, 12]. Then, the applications in materials research (e.g., polymer materials, metal materials, organic proteins, etc.) were developed rapidly. As reported in lots of literatures, thermal analysis plays an important role in evaluating the properties of composite materials (e.g., the mechanisms of crystallization, the denaturation temperature, transition temperature of drug in acidic area, the thermotropic phase behavior of phospholipid, thermodynamic information, clarifying the energetics of macromolecule transitions and in characterizing their thermal stability, the mechanism of entropy-driven process.) [13–19]. In this study, the thermal characteristics of anticancer drug HA–SN and related materials were analyzed with the differential scanning calorimetry (DSC) and thermogravimetry (TG). The DSC method could be used to study the material's enthalpy and glass transition temperatures. For instance, González-Irún Rodríguez et al. [20] studied the effect of silica nanofiller on the glass transition of a polyurethane with DSC. They found the glass transition temperature was not significantly affected by different fillers applied to the polymer, even for different amounts of silica particles, size, and surface treatment when mixed with the polymer. Besides, the TG analyses could be used to measure the mass loss of samples [21, 22].

In this article, we intended to determine whether HA could be encapsulated in SN to form photosensitive drug effectively, with thermal analysis techniques and fluorescence spectrophotometry. Thermal analyses were also applied to characterize the thermal properties of these particles (e.g., HA, SN, HA–M–SN, SN–A–HA, and HA–SN), and evaluate the thermal stability of HA–SN. So far, no reports have been published regarding the characterization of both HA and HA–SN with thermoanalysis.

Materials and experimental methods

System calibration

Differential Scanning Calorimeter (DSC, Perkin-Elmer US, Diamond) and Thermogravimetric Analyzer (TGA, Perkin-Elmer US, Pyris 1) were calibrated with the standard substance Indium (In), Zinc (Zn), Alumel, Perkalloy, Nickel respectively, and the fluorescence spectrometer (Perkin-Elmer, US, LS-50B) was calibrated using standard solution sulfuric acid, quinine sulfate ($\rho = 1.00 \times 10^{-5}$ g/mL, sulfuric acid $C(H_2SO_4) = 0.05$ mol/L) [23–25].

Materials

HA was isolated from the fungus sacs of *Hypocrella bambusae*. The SN, three-aminopropyl triethoxysilane, was purchased from Aldrich Chemical Co., USA. The inclusion complex HA–SN and the silica-nanovector adhered with HA (SN–A–HA) were prepared, as well as the mixture of

HA and SN (M–HA–SN) that was prepared by simply mixing HA with SN.

Experiments

DSC measurement

Samples, each weighing 5–6 mg, of SN, HA, HA–SN, SN–A–HA, and M–HA–SN were taken into the aluminum (Al) pan. Then, the Al pan was sealed, and heated from 25 to 500 °C at 10 °C/min heating rate in argon atmosphere. Meanwhile, the DSC curves were recorded, as shown in Fig. 3.

Thermogravimetric analyzer measurement

Samples, each weighing 5 mg, of SN, HA, HA–SN, SN–A–HA and M–HA–SN samples were taken into the Pt pan, and heated from 25 to 800 °C at 10 °C/min heating rate in nitrogen atmosphere. Meanwhile, TG curves were recorded, as shown in Fig. 4.

Fluorescence spectral measurement

The samples of SN, HA, HA–SN, SN–A–HA were dissolved in double-distilled water. Then, the solution was clarified by sonicating with an ultrasonic cleaner (KuShan Ultrasonic Instrument Co. Ltd., China, KQ3200B). The fluorescence spectra were measured with fluorescence spectrometer: $E_{em} = 480$ nm, scanning from 500 to 800 nm. All the fluorescence spectra were recorded with the same ordinate, and each emission slit was of 5 nm. All spectra were measured at room temperature (25 °C).

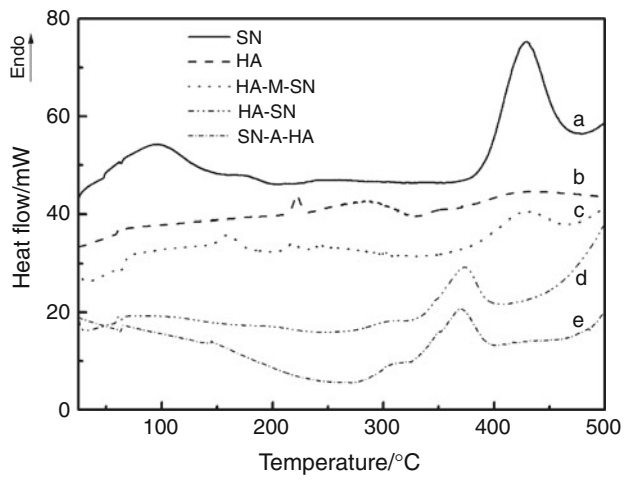

Fig. 3 DSC curves of (*a*) SN, (*b*) HA, (*c*) HA–M–SN, (*d*) HA–SN, and (*e*) SN–A–HA

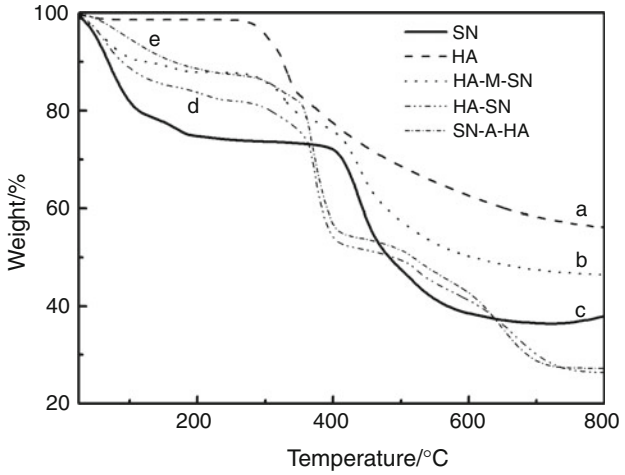

Fig. 4 TG curves of (*a*) HA, (*b*) HA–M–SN, (*c*) SN, (*d*) HA–SN, and (*e*) SN–A–HA

Results and discussion

Silica polymerization mechanism

Silica could be hydrolyzed in alcoholic or aqueous environment. As illustrated in Fig. 5, –R in the structure of SN could be substituted by –OH in the water molecular. Under the alkaline conditions, dehydration and condensation would take place in the silica. Eventually, nanometer particles were compounded which has three-dimensional network structure with the HA encapsulated inside (see Fig. 6). The diameter range of silica particles was about 50–80 nm.

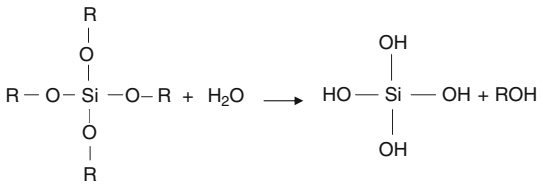

Fig. 5 Silica hydrolysis mechanism

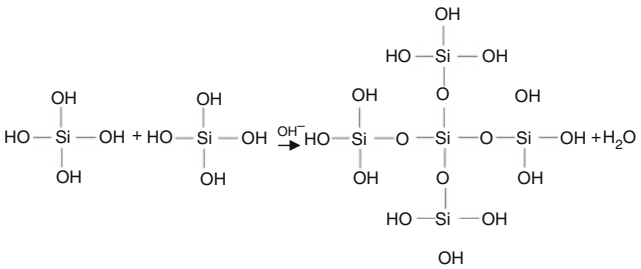

Fig. 6 Silica polymerization mechanism

DSC characterization

The results of measured DSC curves of SN, HA, HA–M–SN, HA–SN, and SN–A–HA are plotted in Fig. 3. There are two peaks observed at 95.13 and 427.93 °C in SN curve (curve a). As we mentioned in Sect. "Silica polymerization mechanism", SN was hydrolyzed in alcoholic or aqueous environment. The reason for the appearance of the former peak is that water or alcohol has been evaporated at 95.13 °C. And the latter peak corresponds to the breakage of –OH and $–NH_2$. HA would melt at 221.93 °C so that an endothermic peak could be observed in curve b (the melting enthalpy can be calculated as 43.45 J/g based on the measurement observed from the HA DSC curve). HA begins to decompose at 328.33 °C which corresponds to the peak indicative of the initiation of exothermic reaction. In the DSC curve of HA–M–SN (curve c), three endothermic peaks appear at 100, 220.13, and 423.53 °C, and one exothermic peak is observed at 327.00 °C. All these four peaks are highly correlated to the corresponding peaks appearing in the SN DSC curve or the HA one, which indicates that the mixture of HA and SN has s non-homophase state. On the contrary, HA–SN curve (curve d) is significantly different from other curves. The latter has only a mild dehydrate endothermic peak at 100 °C nearby, while no peaks could be observed at 221.93, 328.33, or 427.93 °C. On the contrary, in HA–SN curve, a new endothermic peak appears at 373.00 °C, which is higher than the corresponding temperature of HA. Similar endothermic peak can be observed in the curve e (SN–A–HA DSC curve), although it appears at the temperature 5 °C lower than that of HA–SN. The comparison between the endothermic peaks in the DSC curves of HA, HA–SN, and SN–A–HA implies that a new phase might be generated in the HA–SN complex and SN–A–HA due to the formation of the hydrogen band between HA and $–NH_2$. For SN–A–HA, the hydrogen bands are linked between HA particles and $–NH_2$ on the external surface of SN. However, it is speculated that hydrogen bands might be generated between HA particles and $–NH_2$ that lies on the inner surface of SN when HA particles are encapsulated in the SN, since the endothermic peak in the HA–SN curve occurs at the temperature 5 °C higher than that of the SN–A–HA. The different endothermic peaks in HA–SN and SN–A–HA curves also suggests that DSC analysis could be used as an effective tool to determine whether HA particles are encapsulated inside SN or just adhered on its external surface.

TG characterization

Based on TG analysis, we could further determine whether HA is in the core of silica-nanovector or not, and we could also evaluate the thermal stability of HA-loaded silica nanovectors. As shown in Fig. 4, the TG curve of SN (curve c) indicates that the lost weight of SN is 26% when the temperature increases from room temperature to 200 °C. The onset temperature required to initialize the decomposition reaction of SN should be at 414.66 °C with the lost weight of 36.76%, which should correspond to the endothermic reaction peak (at 427.93 °C) in the SN-DSC curve (see Fig. 3). The TG curve of HA (curve a) suggests that a very little loss of alcohol or water would occur when the temperature is lower than 200 °C, since the lost weight is as low as 1.11%. The onset temperature for HA decomposition reaction should be 301.55 °C. As mentioned in Sect. "DSC characterization", HA would melt at 221.93 °C, which is much lower than 301.55 °C. This observation implies that HA would melt first, and then get decomposed. Three weight loss step temperatures in HA–M–SN TG curve (curve b) could be correlated to corresponding feature temperatures observed in the TG curves of SN and HA (as listed in Table 1), which proves that the mixture of SN and HA were formed just by physical mixing.

Moreover, Table 1 shows that the hydrophilicity of HA–SN (curve d) should be better than HA and HA–M–SN, because its lost weight is 17% at the temperature lower than 200 °C, which is larger than the values of HA and HA–M–SN. The HA–SNs decomposition temperature (356.42 °C) is about 55 °C higher than that of HA, and about 18 °C higher than that of SN–A–HA, which is consistent with the results of DSC analyses, which showed that the endothermic temperature of HA–SN is higher than the values of HA and SN–A–HA. It indicates that it might be harder for HA–SN to decompose than both HA and SN–A–HA, which means that the stability of HA–SN should be better than that of HA. The likely explanation might lie in the increased thermal conduction of HA after it was encapsulated in SN. In other words, SN can greatly improve the thermal stability of HA by encapsulating HA in the core. Table 1 also shows that the lost weight of HA–SN (17%) is larger than that of SN–A–HA (13.28%) because, in the HA–SN complex, HA particles are

Table 1 Results of the samples of TG

	SN	HA	HA–M–SN	HA–SN	SN–A–HA
ΔY_1* (%)	26.00	1.11	12.00	17.00	13.28
T_{onset1}** (°C)	414.66	301.55	302.95	356.42	337.93
T_{onset2} (°C)			414.66		

* ΔY_1 was the percent weight loss before 200 °C

** T_{onset1} was the intersection point with the tangent which was obtained from the largest loss weight rate intersected with the baseline, which is the initial temperature of the first decomposition step in TG curves

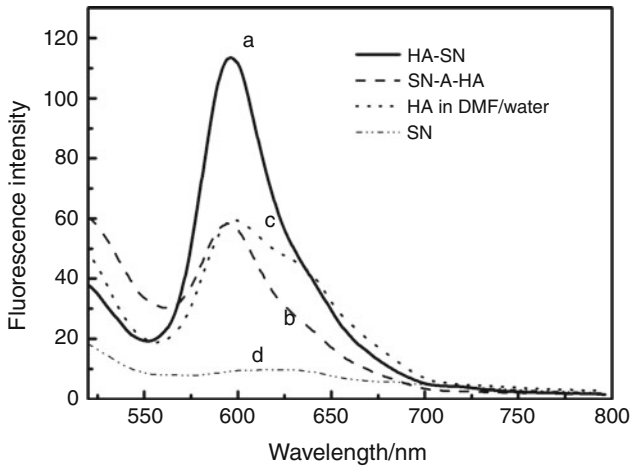

Fig. 7 Emission spectra of: (*a*) HA–SN, (*b*) SN–A–HA, (*c*) HA in DMF/water, and (*d*) SN. The excitation wavelength is 480 nm

encapsulated in SN instead of being adhered on the external surface of SN.

Therefore, the results of TG analyses indicate that HAs can be encapsulated in SNs successfully, and it would result in the improvement of the thermal stability of HA.

Spectroscopic characterization

In order to verify the thermal analysis results, the fluorescence emission spectra (excitation wavelength is 480 nm) of HA–SN, SN–A–HA, HA in DMF/water, and void SN were also measured and plotted in Fig. 7. It is obvious that almost no fluorescence spectrum could be observed for SN within the wavelength range between 520 and 800 nm. And the fluorescence intensity of HA–SN is much stronger than those of free HA and the SN–A–HA. It is speculated that the pure HA and HA–A–SN might stay in a hydrated environment and that the emitted fluorescence could be quenched by water. However, when HA particles were encapsulated in SN, they were located in the inner surface of SN with a hydrophobic environment, which could protect the emitted fluorescence from being quenched. Thus, the results of spectroscopic analysis suggest that HA particles can be encapsulated in SN successfully, which agree with the observations obtained with thermal analysis methods (e.g., DSC and TG).

Conclusions

Thermal technologies (e.g., DSC and TG) were applied to HA, SN, HA–M–HA, SN–A–HA, and HA–SN. The results show that hypocrellin A, a photosensitive drug, could be encapsulated in SN successfully. Fluorescence spectrophotometry was also performed to verify whether HA could be encapsulated in SN. The results of thermal technologies also show that SN could improve the thermal stability of HA, because hydrogen bands might be formed between HA and $-NH_2$ which lies on the inner surface of SN when HA sits in the core of SN. In addition, it shows that the hydrophilicity of HA–SN complex should be better than free HA. This study also verifies that thermal analysis technologies could be used as an effective and rapid tool to determine whether the HA is successfully encapsulated in SN or not, and characterize the properties of the encapsulated HA–SN complex.

Acknowledgements This research was supported by the grants received from the Natural Science Foundation of China (No. 20603018), and the Natural Science Foundation of Jiangsu Province of China (No. BM2007132)

References

1. Roy I, Ohulchanskyy TJ, Pudavar HE, Bergey EJ, Oseroff AR, Morgan J, Dougherty TJ, Prasad PN. Ceramic-based entrapping water-insoluble photosensitizing anticancer drugs: a novel drug-carrier system for photodynamic therapy. J Am Chem Soc. 2003; 125(26):7861–5.
2. Falk H. From the photosensitizer hypericin to the photoreceptor stentorin—the chemistry of phenanthroperylene quinones. Angew Chem Int Ed. 1999;38:3116–36.
3. Diwu ZJ, Lown JW. Hypocrellins and their uses in photosensitization. Photochem Photobiol. 1990;52:609–16.
4. Falk H. From the photosensitizer hypericin to the photoreceptor stentorin—the chemistry of phenanthroperylene quinones. Angew Chem Int Ed. 1999;38:3116–36.
5. Zhou J, Liu J, Xia S, Wang X, Zhang B. Effect of chelation to lanthanum ions on the photodynamic properties of hypocrellin A. J Phys Chem B. 2005;109(41):19529–35.
6. Zhou JH, Wu XH, Wei SH, Gu XT, Feng YY, Wang XS, et al. Raman spectroscopic study of photosensitive damage to lysozyme structure sensitized by hypocrellin A. Spectroscopy. 2006;20(5–6):269–73.
7. Yuying F, Xiaohong W, Jiahong Z, Xiaotian G, Tianhong L, Xuesong W, et al. Study on interaction between hypocrellin A and hemoglobin using spectral methods. Chin J Appl Chem. 2005;22(8):895–8. (in Chinese).
8. Yan F, Kopelman R. The embedding of meta-tetra(hydroxyphenyl)-chlorin into silica nanoparticle platforms for photodynamic therapy and their singlet oxygen production and pH-dependent optical properties. Photochem Photobiol. 2003; 78(6):587–91.
9. Zhou JH, Wu XH, Yang C, Gu XT, Gu T, Zhou L, et al. Spectroscopic studies on the interaction of hypocrellin A with myoglobin. Spectrosc Int J. 2007;21:235–43.
10. Miller GG, Brown K, Ballangrud AM, et al. Preclinical assessment of hypocrellin B and hypocrellin B. derivatives as sensitizer for photodynamic therapy of cancer: progress update. Photochem Photobiol. 1997;65(4):714–22.
11. Wendlandt WWm. Thermal analysis. 3rd ed. New York: Wiley; 1985.
12. Yavlovich A, Singh A, Tarasov S, Capala J, Blumenthal R, Puri A. Design of liposomes containing photopolymerizable phospholipids for triggered release of contents. J Therm Anal Calorim. 2009;98:97–104.

13. Lopez C, Ollivon M. Crystallisation of triacylglycerols in nanoparticles, effect of dispersion and polar lipids. J Therm Anal Calorim. 2009;98:29–37.
14. Lee-Sullivan P, Bettle M. Comparison of enthalpy relaxation between two different molecular masses of a bisphenol-A polycarbonate. J Therm Anal Calorim. 2005;81:169–77.
15. Šesták J, Zámečník J. Can clustering of liquid water and thermal analysis be of assistance for better understanding of biological germplasm exposed to ultra-low temperatures. J Therm Anal Calorim. 2007;88(2):411–6.
16. Bellavia G, Cordone L, Cupane A. Calorimetric study of myoglobin embedded in trehalose–water matrixes. J Therm Anal Calorim. 2009;95(3):699–702.
17. Khvedelidze M, Mdzinarashvili T, Partskhaladze T, Nafee N, Schaefer UF, Lehr C-M, Schneider M. Calorimetric and spectrophotometric investigation of PLGA nanoparticles and their complex with DNA. J Therm Anal Calorim. 2009. doi:10.1007/s10973-009-0137-x.
18. Pentak D, Su_kowski WW, Su_kowska A. Calorimetric and Epr studies of the thermotropic phase behavior of phospholipid membranes. J Therm Anal Calorim. 2008;93(2):471–7.
19. Giancola C. A convenient tool for studying the stability of proteins and nucleic acids. Differential scanning calorimetry. J Therm Anal Calorim. 2008;91(1):79–85.
20. González-Irún Rodríguez J, Carreira P, García-Diez A, Hui D, Artiagaand R, Liz-Marzán LM. Nanofiller effect on the glass transition of a polyurethane. J Therm Anal Calorim. 2007;87(1):45–7.
21. Gabelical Z, Charmot A, Vataj R, Soulimane R, Barrault J, Valange S. Thermal degradation of iron chelate complexes adsorbed on mesoporous silica and alumina. J Therm Anal Calorim. 2009;95(2):445–54.
22. Markovska IG, Lyubchev LA. A study on the thermal destruction of rice husk in air and nitrogen atmosphere. J Therm Anal Calorim. 2007;89(3):809–14.
23. ASTM E794-81: Standard test method for melting temperatures and crystallization temperatures by thermal analysis.
24. ASTM E914-83: Standard test method for practice for evaluating temperature scale for thermogravity.
25. Zhongmin L. The general analysis and measurement test order of Modern analytical instruments. Beijing, China: Science and Technology Literature Publishing House; 1997.